Asian Journal of Chemistry; Vol. 38, No. 3 (2026), 781-791
ASIAN JOURNAL OF CHEMISTRY
https://doi.org/10.14233/ajchem.2026.35442

Synthesis and Molecular Docking Studies of Benzimidazole Hybrids Incorporating 1,3,4-Oxadiazole, 1,2,4-Triazole and Schiff Base as Potential Antibreast Cancer Agents

B. CHANDRASHEKHARA KUMAR[1,*], RAJA RAJESHWARI[2], T.S. KESHAVA PRASAD[3], ARUN BHAGWATH[1] and SUMANGALA RAO[1]

[1]The Yenepoya Institute of Arts, Science, Commerce and Management, The Yenepoya (Deemed to be university), Mangalore-575013, India
[2]Department of Surgical Oncology, Yenepoya Medical College, Yenepoya (Deemed to be University), Mangalore-575018, India
[3]Center for Systems Biology and Molecular Medicine, Yenepoya Research Centre, Yenepoya (Deemed to be University), Mangalore-575018, India

*Corresponding author: E-mail: chandrashekhar@yenepoya.edu.in

Received: 12 December 2025 *Accepted*: 4 February 2026 *Published online*: 6 March 2026 AJC-22298

A series of new benzimidazole-based hybrid compounds were synthesised by incorporating Schiff bases, 1,2,4-triazoles and 1,3,4-oxadiazoles and were evaluated for breast anticancer activity using molecular docking, MD simulations and ADME studies. The benzimidazole-based hybrid compounds were prepared through functionalisation of the benzimidazole scaffold *via* *N*-acylation, conversion to hydrazides and subsequent cyclisation to form 1,3,4-oxadiazoles and 1,2,4-triazoles. Molecular docking, MD simulations and ADME predictions were performed to assess anticancer potential particularly against breast-cancer-related targets. The oxadiazole hybrid (**5e**) showed moderate binding to β-tubulin suggesting the inhibition of microtubule function. Triazole derivatives (**7a**, **7b**) exhibited high binding affinity to caspase-3 and PARP-1, which indicates pro-apoptotic and DNA repair inhibitory effects respectively. The Schiff base derivative (**9a**) demonstrated strong binding to ERα suggesting modulation of the hormone pathway. MD simulations demonstrated stable ligand-protein interactions and ADME analysis suggested good drug-likeness and oral absorption.

Keywords: Benzimidazole, 1,2,4-Triazoles, Schiff bases, 1,3,4-Oxadiazoles, Antibreast cancer, Molecular docking.

INTRODUCTION

Breast cancer remains a major global health concern with triple-negative breast cancer (TNBC) representing a highly aggressive form lacking effective targeted therapies. This challenge has intensified interest in multi-targeted heterocyclic compounds supported by network-based and computational insights into tumor heterogeneity [1,2]. Benzimidazole is a privileged scaffold with notable antiproliferative and DNA binding activities [3-7]. Complementary pharmacophores such as 1,3,4-oxadiazoles and 1,2,4-triazoles exhibit anticancer and apoptosis-inducing potential [8], while Schiff bases provide receptor-selective properties [9-12].

The present study reports a distinct class of benzimidazole based hybrids developed through a divergent synthetic strategy rather than direct heterocycle coupling commonly described in earlier reports *i.e.*, benzimidazole scaffold can be incorporated with heterocyclic units *via* *N*-acylation and hydrazide formation enabling subsequent cyclisation into 1,3,4-oxadiazole or 1,2,4-triazole moieties from a common intermediate. Moreover, the introduction of Schiff base linkages provides enhanced structural and electronic diversity. This approach expands the chemical space of benzimidazole hybrids and offers a versatile platform for the systematic structure-activity relationship investigations.

EXPERIMENTAL

All reagents and solvents were procured from reputed chemical suppliers (Merck, Loba, Sigma-Aldrich) as analytical grade materials and used without further purification. The reaction progress was monitored by thin-layer chromatography (TLC) on Merck silica gel 60 F_{254} plates, visualised under UV light or in an iodine chamber. Melting points were determined in open capillaries on a Labtronics Digital Melting Point apparatus (Model LT-115) and are uncorrected. FTIR spectra

This is an open access journal, and articles are distributed under the terms of the Attribution 4.0 International (CC BY 4.0) License. This license lets others distribute, remix, tweak, and build upon your work, even commercially, as long as they credit the author for the original creation. You must give appropriate credit, provide a link to the license, and indicate if changes were made.

(4000-400 cm^{-1}) were recorded on a Bruker FTIR spectrophotometer. ^1H and ^{13}C NMR spectra were acquired on a Bruker Avance III 400 MHz spectrometer (400 MHz for ^1H and 75 MHz for ^{13}C).

Synthesis of 1,3,4-oxadiazole derivatives (5a-g): In a 250 mL round-bottom flask, an equimolar mixture of 2-substituted benzimidazole derivatives (**1a-g**) (0.1 mol) and ethyl chloroacetate (**2**) (0.1 mol) in 200mL acetone was refluxed with acetone for 24 h in the presence of potassium carbonate. The solvent was distilled off to obtain the methyl[2-substituted-1*H*-benzimidazol-1-yl] acetate derivatives (**3a-g**).

Compounds (**3a-g**) were refluxed with hydrazine hydrate (0.1 mol) in 100 mL of ethanol for 14 h, yielding 2-[2-substituted-1*H*-benzimidazol-1-yl]acetohydrazide derivatives (**4a-g**). The reaction mixture was allowed to cool to room temperature, leading to the formation of product in the reflux flask. The solid was then filtered, dried and recrystallized from ethanol.

Synthesis of 5-(1*H*-benzimidazol-1-ylmethyl)-1,3,4-oxadiazole-2-thiol derivatives (5a-g): A series of 5-[(2-substituted-1*H*-benzimidazol-1-yl)methyl]-1,3,4-oxadiazole-2-thiol derivatives (**5a-g**) were obtained by refluxing 2-[2-substituted-1*H*-benzimidazol-1-yl]acetohydrazide derivatives (**4a-g**) (0.1 mol) with the CS_2-alcoholic KOH (0.15 mol) in 150 mL ethanol. The products were filtered, washed with water and dried. further purified by recrystallisation from ethanol (**Scheme-I**).

5-(1*H*-Benzimidazol-1-ylmethyl)-1,3,4-oxadiazole-2-thiol (5a): Yield: 51%, m.p.: 157-159 ºC; IR (KBr, ν_{max}, cm^{-1}): 3062.75 (Ar C–H), 2954.74 (aliphatic C–H), 2560.57 (S–H), 1638.67 (C=N), 1589.23 (C=C), 1226.64 (C–O), 750.06 (C–S); ^1H NMR (DMSO-d_6) δ ppm: 4.79 (s, 1H, SH), 5.73(s, 2H, CH_2), 6.87-8.12 (m, 5H, Ar-H); EI-MS 233.26 (M+1). Elemental analysis of $C_{10}H_8N_4OS$: Calcd. (found) %: C, 48.38 (48.62); H, 4.31 (4.50); N, 24.13 (24.15).

1-[(5-Sulfanyl-1,3,4-oxadiazol-2-yl)methyl]-1*H*-benzimidazol-2-ol (5b): Yield: 56%, m.p.: 177-179 ºC; IR (KBr, ν_{max}, cm^{-1}): 3502.49 (O–H), 3047.32 (Ar C–H), 2846.17 (aliphatic C–H), 2560.72 (S–H), 1620.09 (C=N), 1573.81 (C=C), 1272.93 (C–O), 732.90 (C–S); ^1H NMR (DMSO-d_6) δ ppm: 4.79 (s, 1H, SH), 5.33 (s, 2H, CH_2), 6.87-7.72 (m, 4H, Ar-H), 11.13 (s, 1H, OH). EI-MS 249.26 (M+1). Elemental analysis of $C_{10}H_8N_4O_2S$: Calcd. (found) %: C, 48.38 (48.52); H, 3.22 (3.70); N, 22.13 (22.01).

5-[(2-Methoxy-1*H*-benzimidazol-1-yl)methyl]-1,3,4-oxadiazole-2-thiol (5c): Yield: 76%, m.p.: 260-262 ºC; IR (KBr, ν_{max}, cm^{-1}): 3090.07 (Ar C–H), 2870.00 (aliphatic C–H), 2540.12 (S–H), 1620.11 (C=N), 1580.77 (C=C), 1270.67 (C–O), 738.07 (C–S); ^1H NMR (DMSO-d_6) δ ppm: 3.87 (s, 3H, OCH_3), 4.79 (s, 1H, SH), 5.37 (s, 2H, CH_2), 6.85-7.79 (m, 4H, Ar-H). EI-MS 263.28 (M+1); Elemental analysis of $C_{11}H_{10}N_4O_2S$: Calcd. (found) %: C, 50.38 (49.97); H, 3.81 (3.87); N, 21.37 (21.79).

5-[(2-Nitro-1*H*-benzimidazol-1-yl)methyl]-1,3,4-oxadiazole-2-thiol (5d): Yield: 72%, m.p.: 271-273 ºC; IR (KBr, ν_{max}, cm^{-1}): 3100.67 (Ar C–H), 2881.32 (aliphatic C–H), 2537.03 (S–H), 1620.01 (C=N), 1530.76 (C=C), 1550.15, 1350.67 (N–O), 1275.67 (C–O), 735.97 (C–S); ^1H NMR (DMSO-d_6) δ ppm: 4.79 (s, 1H, SH), 5.35 (s, 2H, CH_2), 6.84-7.80 (m, 4H, Ar-H). EI-MS 278.25 (M+1); Elemental analysis of $C_{11}H_{10}N_4O_2S$: Calcd. (found) %: C, 50.38 (49.97); H, 3.81 (3.87); N, 21.37 (21.79).

5-[(2-Fluoro-1*H*-benzimidazol-1-yl)methyl]-1,3,4-oxadiazole-2-thiol (5e): Yield: 70%, m.p.: 199-201 ºC; IR (KBr, ν_{max}, cm^{-1}): 738.77 (C–S), 1210.17 (C–F), 1277.88 (C–O), 1552.37 (C=C), 1604.12 (C=N), 2517.17 (S–H), 2860.00 (aliph. C–H), 3107.12 (Ar C–H). ^1H NMR (DMSO-d_6) δ ppm: 4.79 (s, 1H, SH), 5.35 (s, 2H, CH_2), 6.87-7.57 (m, 4H, Ar-H); EI-MS 251.25 (M+1); Elemental analysis of $C_{10}H_7N_4OSF$: Calcd. (found) %: C, 48.00 (49.71); H, 2.80 (2.71); N, 22.40 (22.40).

5-[(2-Chloro-1*H*-benzimidazol-1-yl)methyl]-1,3,4-oxadiazole-2-thiol (5f): Yield: 70%, m.p.: 131-133 ºC; IR (KBr, ν_{max}, cm^{-1}): 737.58 (C–S), 757.56 (C–Cl), 1278.77 (C–O), 1517.02 (C=C), 1618.17 (C=N), 2517.25 (S–H), 2860.00 (aliph. C–H), 3107.45 (Ar C–H). ^1H NMR (DMSO-d_6) δ ppm: 4.79 (s, 1H, SH), 5.35 (s, 2H, CH_2), 6.87-7.57 (m, 4H, Ar-H); EI-MS 268.70 (M+2); Elemental analysis of $C_{10}H_7N_4OSCl$: Calcd. (found) %: C, 45.11 (44.71); H, 2.62 (2.61); N, 21.05 (21.40).

5-[(2-Bromo-1*H*-benzimidazol-1-yl)methyl]-1,3,4-oxadiazole-2-thiol (**5g):** Yield: 70%, m.p.: 201-203 ºC; IR (KBr, ν_{max}, cm^{-1}): 560.57 (C–Br), 735.57 (C–S), 1270.17 (C–O), 1552.09 (C=C), 1617.06 (C=N), 2517.07 (S–H), 2860.77 (aliphatic C–H), 3107.12 (Ar C–H). ^1H NMR (DMSO-d_6) δ ppm: 4.79 (s, 1H, SH), 5.31 (s, 2H, CH_2), 6.87-7.57 (m, 4H, Ar-H); EI-MS 313.15 (M+2); Elemental analysis of $C_{10}H_7N_4OSBr$: Calcd. (found) %: C, 38.58 (39.71); H, 2.25 (2.21); N, 18.00 (18.40).

Synthesis of 4-amino-5-(1*H*-benzimidazol-1-ylmethyl)-4*H*-1,2,4-triazole-3-thiol derivatives (7a-g): 2-(1*H*-Benzimidazol-1-ylacetyl)hydrazinecarbodithioic acid derivatives (**6a-g**) were obtained by stirring 2-(2-substituted-1*H*-benzimidazol-1-yl)acetohydrazide (**4a-g**) with CS_2 (0.15 mol) and alcoholic KOH for 24 h. The resulting salt-like product was air-dried in a desiccator for two days. Subsequently, the dried products were mixed with hydrazine hydrate (0.1 mol) in a

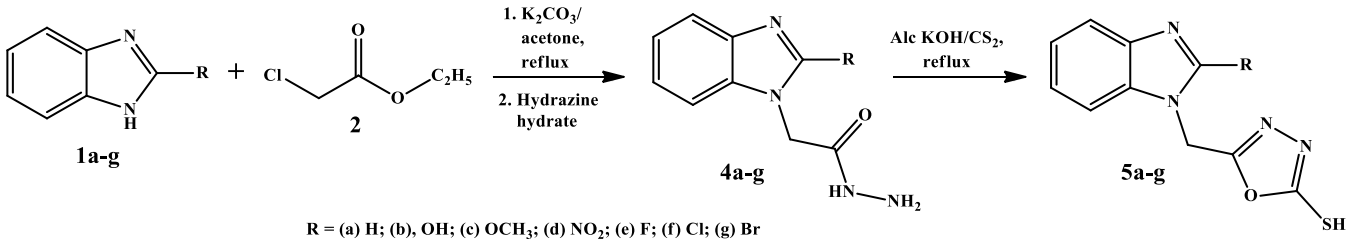

Scheme-I: Synthesis of 5-(1*H*-benzimidazol-1-ylmethyl)-1,3,4-oxadiazole-2-thiol derivatives (**5a-g**)

round-bottom flask and refluxed for 12 h to obtain triazole derivatives. After completion of the reaction, the reaction mixture was poured into a slightly acidic solution to yield 4-amino-5-(1*H*-benzimidazol-1-ylmethyl)-4*H*-1,2,4-triazole-3-thiol derivatives (**7a-g**) (**Scheme-II**). The products were further purified by recrystallisation from ethanol.

4-Amino-5-(1*H*-benzimidazol-1-ylmethyl)-4*H*-1,2,4-triazole-3-thiol (7a): Yield: 75%, m.p.: 189-191 ºC; IR (KBr, ν_{max}, cm^{-1}): 3456.20, 3433.06 (N–H *str*.), 3047.32 (Ar C–H), 2923.88 (aliphatic C–H), 2570.00 (S–H), 1620.09 (C=N), 1573.81 (C=C), 748.33 (C–S); ^{1}H NMR (DMSO-d_6) δ ppm: 4.79 (s, 1H, SH), 5.33 (s, 2H, CH_2), 6.87-7.87 (m, 5H, Ar-H), 7.86 (s, 2H, NH_2); EI-MS 247.29 (M+1); Elemental analysis of $C_{10}H_{10}N_6S$: Calcd. (found) %: C, 48.78 (48.71); H, 4.06 (4.51); N, 34.14 (34.40).

1-[(4-Amino-5-sulfanyl-4*H*-1,2,4-triazol-3-yl)methyl]-1*H*-benzimidazol-2-ol (7b): Yield: 70%, m.p.: 192-194 ºC; IR (KBr, ν_{max}, cm^{-1}): 3641.35 (O–H), 3448.49, 3317.34 (N–H *str*.), 3024.18 (Ar C–H), 2947.03 (aliphatic C–H), 2570.00 (S–H), 1596.85 (C=N), 1527.22 (C=C), 1255.72 (C–O), 756.04 (C–S); ^{1}H NMR (DMSO-d_6) δ ppm: 4.79 (s, 1H, SH), 5.35 (s, 2H, CH_2), 6.87-7.88 (m, 4H, Ar-H), 8.27 (s, 2H, NH_2), 11.79 (s, 1H, OH). EI-MS 263.29 (M+1); Elemental analysis of $C_{10}H_{10}N_6OS$: Calcd. (found) %: C, 47.80 (46.71); H, 3.81 (3.71); N, 32.06 (32.40).

4-Amino-5-[(2-methoxy-1*H*-benzimidazol-1-yl)methyl]-4*H*-1,2,4-triazole-3-thiol (7c): Yield: 64%, m.p.: 194-196 ºC; IR IR (KBr, ν_{max}, cm^{-1}): 3423.49, 3354.34 (N–H), 3025.18 (Ar C–H), 2860.10 (aliphatic C–H), 2570.00 (S–H), 1596.95 (C=N), 1527.52 (C=C), 1257.67 (C–O), 753.04 (C–S); ^{1}H NMR (DMSO-d_6) δ ppm: 3.87 (s,3H, OCH_3), 4.77 (s, 1H, SH), 5.35 (s, 2H, CH_2), 8.29 (s, 2H, NH_2), 6.87-7.57 (m, 4H, Ar-H); EI-MS 277.31 (M+1); Elemental analysis of $C_{11}H_{12}N_6OS$: Calcd. (found) %: C, 48.00 (47.71); H, 4.36 (4.51); N, 33.43 (33.40).

4-Amino-5-[(2-nitro-1*H*-benzimidazol-1-yl)methyl]-4*H*-1,2,4-triazole-3-thiol (7d): Yield: 59%, m.p.: 193-195 ºC; IR (KBr, ν_{max}, cm^{-1}): 3423.49, 3350.16 (N–H), 3107.23 (Ar C–H), 2860.27 (aliphatic C–H), 2557.32 (S–H), 1600.03 (C=N), 1550.09 (asym N-O), 1528.54 (C=C), 760.08 (C–S); ^{1}H NMR (DMSO-d_6) δ ppm: 4.79 (s, 1H, SH), 5.37(s, 2H, CH_2), 8.27 (s, 2H, NH_2), 6.87-7.57 (m, 4H, Ar-H); EI-MS 292.28 (M+1); Elemental analysis of $C_{10}H_9N_7O_2S$: Calcd. (found) %: C, 41.23 (40.71); H, 3.09 (3.51); N, 33.67 (33.40).

4-Amino-5-[(2-fluoro-1*H*-benzimidazol-1-yl)methyl]-4*H*-1,2,4-triazole-3-thiol (7e): Yield: 62%, m.p.: 201-203 ºC; IR (KBr, ν_{max}, cm^{-1}): 3443.49, 3248.00 (N–H), 3050.05 (Ar C–H), 2850.00 (aliphatic C–H), 2550.17 (S–H), 1627.32 (C=N), 1532.65 (C=C), 1050.00 (C–F), 750.23 (C–S); ^{1}H NMR (DMSO-d_6) δ ppm: 4.78 (s, 1H, SH), 5.32 (s, 2H, CH_2), 8.25 (s, 2H, NH_2), 6.84-7.77 (m, 4H, Ar-H); EI-MS 265.28 (M+1); Elemental analysis of $C_{10}H_9N_6SF$: Calcd. (found) %: C, 45.45 (46.71); H, 3.04 (3.51); N, 31.93 (31.40).

4-Amino-5-[(2-chloro-1*H*-benzimidazol-1-yl)methyl]-4*H*-1,2,4-triazole-3-thiol (7f): Yield: 69%, m.p.: 202-204 ºC; IR (KBr, ν_{max}, cm^{-1}): 3443.49, 3248.08 (N–H), 2850.01 (aliphatic C–H), 2550.15 (S–H), 1627 (C=N), 1534.67 (C=C), 1305.14 (Ar C–H), 750.17 (C–Cl); ^{1}H NMR (DMSO-d_6) δ ppm: 4.75 (s, 1H, SH), 5.36 (s, 2H, CH_2), 8.28 (s, 2H, NH_2), 6.84-7.77 (m, 4H, Ar-H). EI-MS 282.73 (M+2); Elemental analysis of $C_{10}H_9N_6SCl$: Calcd. (found) %: C, 42.85 (42.71); H, 3.21 (3.51); N, 30.00 (30.40).

4-Amino-5-[(2-bromo-1*H*-benzimidazol-1-yl)methyl]-4*H*-1,2,4-triazole-3-thiol (7g): Yield: 70%, m.p.: 203-205 ºC; IR (KBr, ν_{max}, cm^{-1}): 3450.49, 3248.07 (N–H), 3050.16 (Ar C–H), 2850.00 (aliphatic C–H), 2550.07 (S–H), 1627.45 (C=N), 1532.05 (C=C), 1150.11 (C–Br), 750.27 (C–S); ^{1}H NMR (DMSO-d_6) δ ppm: 4.77 (s, 1H, SH), 5.37 (s, 2H, CH_2), 8.29 (s, 2H, NH_2), 6.84-7.77 (m, 4H, Ar-H); EI-MS 327.18 (M+2); Elemental analysis of $C_{10}H_9N_6SBr$: Calcd. (found) %: C, 36.92 (35.71); H, 2.76 (2.51); N, 25.84 (25.40).

Synthesis of 5-(1*H*-benzimidazol-1-ylmethyl)-4-[(*E*)-benzylideneamino]-4*H*-1,2,4-triazole-3-thiol derivatives (9a-g): 4-Amino-5-(1*H*-benzimidazol-1-ylmethyl)-4*H*-1,2,4-triazole-3-thiol derivatives (**7a-g**) were refluxed with substituted aromatic aldehydes (0.1 mol) (**8**) in ethanol for ~10 h, catalysed by a few drops of conc. H_2SO_4 (**Scheme-III**). Recrystallisation was done for the synthesised compounds to obtain pure compounds using partially diluted solvents such as ethanol,

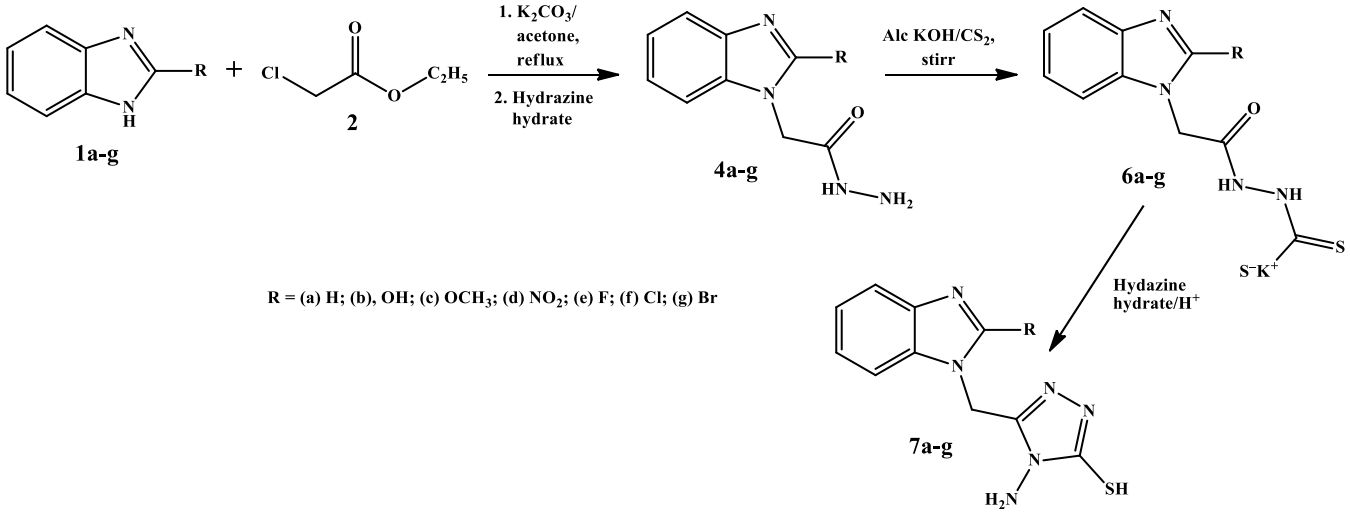

Scheme-II: Synthesis of 4-amino-5-(1*H*-benzimidazol-1-ylmethyl)-4*H*-1,2,4-triazole-3-thiol derivatives (**7a-g**)

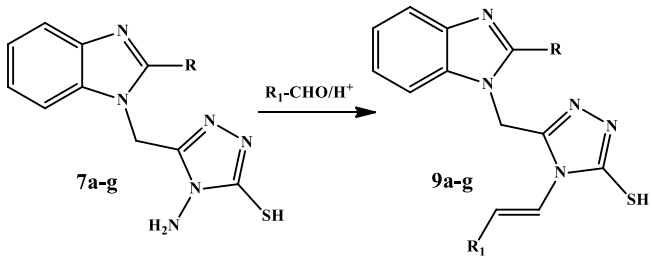

R = (a) H; (b), OH; (c) OCH_3; (d) NO_2; (e) F; (f) Cl; (g) Br
R_1 = (a) C_6H_5; (b) C_6H_5-CH_3; (c) C_6H_5-OCH_3; (d) C_6H_5-NO_2; (e) C_6H_5-F; (f) C_6H_5-Cl; (g) C_6H_5-Br

Scheme-III: Synthesis of 5-(1*H*-benzimidazol-1-ylmethyl)-4-[(*E*)-benzylideneamino]-4*H*-1,2,4-triazole-3-thiol derivatives (**9a-g**)

methanol or higher members of alcohols based on the polarity of solvents.

5-(1*H*-Benzimidazol-1-ylmethyl)-4-[(*E*)-benzylideneamino]-4*H*-1,2,4-triazole-3-thiol (9a): Yield: 64%, m.p.: 191-194 ºC; IR (KBr, ν_{max}, cm^{-1}): 3050.00 (Ar C–H), 2950.17 (aliphatic C–H), 1640.95 (imine C=N), 1596.95, 1434.94 (Ar C=C), 756.04 (C–S); ^{1}H NMR (DMSO-d_6) δ ppm: 5.25 (s, 2H, CH_2), 7.87 (s, 1H, CH), 6.87-8.79 (m, 10H, Ar-H), 9.73 (s, 1H, SH); EI-MS 335.39 (M+1); Elemental analysis of $C_{17}H_{14}N_6S$: Calcd. (found) %: C, 38.58 (37.71); H, 2.25 (2.51); N, 18.00 (18.40).

1-[(4-{(*E*)-[(4-Methylphenyl)imino]methyl}-5-sulphanyl-4*H*-1,2,4-triazol-3-yl)methyl]-1*H*-benzimidazol-2-ol (9b): Yield: 79%, m.p.: 195-197 ºC; IR (KBr, ν_{max}, cm^{-1}): 680.83 (C–S), 1251.72 (C–O), 1560.30 (C=C), 1596.95 (Ar C=N), 1650.95 (imine C=N) 2854.45 (aliphatic C–H), 3022.25 (Ar C–H), 3390.63 (O–H). ^{1}H NMR (DMSO-d_6) δ ppm: 2.42 (s, 3H, CH_3) 5.23 (s, 2H, CH_2), 7.85 (s, 1H, CH), 6.87-8.81 (m, 8H, Ar-H), 9.73 (s, 1H, SH), 12.68 (s, 1H, OH); EIMS 365.42 (M+1); Elemental analysis of $C_{18}H_{16}N_6OS$: Calcd. (found) %: C, 36.54 (36.71); H, 2.71 (2.62); N, 17.17 (17.39).

5-[(2-Methoxy-1*H*-benzimidazol-1-yl)methyl]-4-{(*E*)-[(4-methoxyphenyl)imino]methyl}-4*H*-1,2,4-triazole-3-thiol (9c): Yield: 78%, m.p.: 194-196 ºC; IR (KBr, ν_{max}, cm^{-1}): 3022.25 (Ar C–H), 2854.45 (aliphatic C–H), 1650.95 (imine C=N), 1586.95 (Ar C=N), 1550.30 (C=C), 1257.72 (C–O), 720.83 (C–S); ^{1}H NMR (DMSO-d_6) δ ppm: 3.87 (s, 6H, OCH_3) 5.27 (s, 2H, CH_2), 7.82 (s, 1H, CH), 6.87-8.23 (m, 8H, Ar-H), 9.73 (s, 1H, SH); EI-MS 395.45 (M+1); Elemental analysis of $C_{19}H_{18}N_6O_2S$: Calcd. (found) %: C, 59.50 (58.50); H, 4.40 (4.00); N, 23.14 (23.17).

5-[(2-Nitro-1*H*-benzimidazol-1-yl)methyl]-4-{(*E*)-[(4-nitrophenyl)imino]methyl}-4*H*-1,2,4-triazole-3-thiol (9d): Yield: 74%, m.p.: 235-237 ºC; IR (KBr, ν_{max}, cm^{-1}): 3050.00 (Ar C–H), 2950.17 (aliphatic C–H), 1640.95 (imine C=N), 1596.95, 1434.94 (Ar C=C), 1420 (N-O), 756.04 (C–S); ^{1}H NMR (DMSO-d_6) δ ppm: 5.23 (s, 2H, CH_2), 7.82 (s, 1H, CH), 6.87-8.67 (m, 8H, Ar-H), 9.75 (s, 1H, SH). EIMS 425.39 (M+1); Elemental analysis of $C_{17}H_{12}N_8O_4S$: Calcd. (found) %: C, 53.82 (53.62); H, 3.43 (3.03); N, 23.85 (23.85).

5-[(2-Fluoro-1*H*-benzimidazol-1-yl)methyl]-4-{(*E*)-[(4-fluorophenyl)imino]methyl}-4*H*-1,2,4-triazole-3-thiol (9e): Yield: 76%, m.p.: 193-195 ºC; IR (KBr, ν_{max}, cm^{-1}): 3022.25 (Ar C–H), 2854.45 (aliphatic C–H), 1650.95 (imine C=N), 1596.95 (Ar C=N), 1560.30 (C=C), 1150 (C-F), 720.83 (C–S); ^{1}H NMR (DMSO-d_6) δ ppm: 5.23 (s, 2H, CH_2), 7.85 (s, 1H, CH), 6.87-8.75 (m, 8H, Ar-H), 9.77 (s, 1H, SH); EI-MS 371.37 (M+1); Elemental analysis of $C_{17}H_{12}N_6SF_2$: Calcd. (found) %: C, 57.95 (56.95); H, 3.69 (3.17); N, 23.86 (23.86).

5-[(2-Chloro-1*H*-benzimidazol-1-yl)methyl]-4-{(*E*)-[(4-chlorophenyl)imino]methyl}-4*H*-1,2,4-triazole-3-thiol (9f): Yield: 75%, m.p.: 192-194 ºC; IR (KBr, ν_{max}, cm^{-1}): 3022.25 (Ar C–H), 2854.45 (aliphatic C–H), 1650.95 (imine C=N), 1596.95 (Ar C=N), 1560.30 (C=C), 700 (C–Cl), 680.83 (C–S); ^{1}H NMR (DMSO-d_6) δ ppm: 5.27 (s, 2H, CH_2), 7.85 (s, 1H, CH), 6.87-8.75 (m, 8H, Ar-H), 9.78 (s, 1H, SH); EI-MS 405.28 (M+2); Elemental analysis of $C_{17}H_{12}N_6SCl_2$: Calcd. (found) %: C, 55.43 (54.73); H, 3.53 (3.13); N, 22.82 (22.32).

5-[(2-Bromo-1*H*-benzimidazol-1-yl)methyl]-4-{(*E*)-[(4-bromophenyl)imino]methyl}-4*H*-1,2,4-triazole-3-thiol (9g): Yield: 74%, m.p.: 191-193 ºC; IR (KBr, ν_{max}, cm^{-1}): 3022.25 (Ar C–H), 2854.45 (aliphatic C–H), 1650.95 (imine C=N), 1596.95 (Ar C=N), 1560.30 (C=C), 690 (C–Br), 680.83 (C–S); ^{1}H NMR (DMSO-d_6) δ ppm: 5.23 (s, 2H, CH_2), 7.85 (s, 1H, CH), 6.87-8.85 (m, 8H, Ar-H), 9.75 (s, 1H, SH). EIMS 494.19 (M+2); Elemental analysis of $C_{17}H_{12}N_6SBr_2$: Calcd. (found) %: C, 49.39 (48.89); H, 3.14 (3.01); N, 20.33 (20.32).

Integrated strategy for selecting targets for computational work-network pharmacology component: In order to rationalise target selection for each class of synthesised heterocycles this study employed an integrated technique that coupled literature-based mechanistic mapping with *in silico* modelling. The method made sure that docking and MD simulations were both physiologically relevant and mechanistically justifiable by matching drug classes with their most likely biological mechanisms and verified protein targets. The interpretability and reliability of all computational results were enhanced by the compound-class-to-target mapping [13-17].

Mechanistic correlation with breast cancer subtypes: The cytotoxicity was evaluated in MCF-7 (ER^+) and MDA-MB-231 (TNBC) cell lines to confirm the mechanistic mapping of each chemical class to breast cancer subtypes. Schiff base derivatives were connected to ERα regulation in MCF-7 cells, triazole hybrids to apoptosis mediated by caspase and PARP in MDA-MB-231 and oxadiazole hybrids to disruption of microtubule dynamics caused by β-tubulin.

Strategic integration of mechanistic and computational workflows: The mechanistic mapping enhanced the biological relevance of the *in silico* workflow, which integrated target-specific docking (Glide), molecular dynamics simulations and ADME/toxicity predictions (QikProp). These analyses enhanced the biological interpretability and target relevance of the computational results as well as the anticancer potential of the synthesized hybrids.

Computational modeling: To prepare low-energy 3D conformers at physiological pH, ligands **5g**, **7g** and **9g** were synthesised in Maestro (Schrödinger 2020-3) using LigPrep with the OPLS-4 force field. After being obtained from the RCSB, the target proteins–β-tubulin (1SA0), caspase-3 (1PAU),

PARP-1 (4R6E) and ERα (3ERT), were processed using the protein preparation wizard (hydrogen addition, water removal and OPLS-4 minimisation). Flexible ligand docking was carried out in Glide-SP and receptor grids were developed around the active site identified by SiteMap. The ligand interaction pose was used to analyse top-scoring poses and then 100 ns Desmond MD simulations (OPLS-4, TIP3P, NPT) were used to assess interaction persistence and structural stability. QikProp was used to predict ADME features such as logP, solubility, permeability, metabolic liability and Lipinski compliance.

***In vitro* cytotoxicity assay:** The cytotoxic activity of compounds **5e**, **7a**, **7b** and **9a** was evaluated using a standard MTT/MTS assay. Cells were seeded into 96-well plates, incubated overnight (37 ºC, 5% CO_2) and treated with increasing concentrations of the test compounds (final DMSO ≤ 0.1% v/v). The untreated and vehicle-treated cells served as controls. After 24-48 h incubation, the assay reagent was added and absorbance was recorded using a microplate reader. The cell viability was expressed relative to controls and IC_{50} values were calculated by nonlinear regression. All experiments were performed in triplicate and expressed as mean ± SD.

RESULTS AND DISCUSSION

Two series of benzimidazole-based heterocyclic derivatives namely 1,3,4-oxadiazoles (**5a-g**) 1,2,4-triazoles (**7a-g**) and Schiff bases (**9a-g**) were synthesised as outlined in **Schemes I-III**. The first step of the synthetic route involved the reaction of 2-substituted benzimidazole derivatives (**1a-g**) with ethyl chloroacetate (**2**) in the presence of K_2CO_3 in acetone as solvent, which afforded methyl (2-substituted-1*H*-benzimidazol-1-yl) acetate derivatives (**3a-g**) in good yields. Subsequently these intermediates (**3a-g**) were treated with hydrazine hydrate to yield 2-(1*H*-benzimidazol-1-yl)acetohydrazide derivatives (**4a-g**). These hydrazide intermediates were utilised as versatile precursors for further transformations under two different synthetic conditions.

Computational studies: The benzimidazole-based hybrids showed moderate to strong affinities for all four biological targets according to molecular docking with Glide scores ranging from -4.11 to -6.85 kcal mol^{-1} (Table-1). Through peripheral polar and van der Waals contacts (ASN101, THR145, VAL171, ASP179), the oxadiazole hybrids connected to β-tubulin (1SA0) with a moderate affinity (-4.11 kcal mol^{-1}) (Fig. 1a) indicating partial occupation of the microtubule interface. Hydrogen bonds (SER343, ARG341) and π–π stacking (TYR338, TRP340) were generated by the triazole–caspase-3 complex (1PAU) (Fig. 1b) suggesting the possibility of inducing apoptosis by caspase activation. Similar to this, the triazole–PARP-1 complex (4R6E) exhibited strong binding (-6.31 kcal mol^{-1}) stabilised by π–π stacking (TRP861, TYR896, PHE897) and hydrogen bonding (SER904, GLY863, HIS862) (Fig. 1c). With minimal polar contacts (THR347, GLU353) and dense hydrophobic packing (LEU349, LEU391, MET388), the Schiff base derivative that targets ERα (3ERT) showed the maximum affinity (-6.85 kcal mol^{-1}) (Fig. 1d-b). These findings show the structural adaptability of the benzimidazole scaffold wherein Schiff base derivatives oxadiazole and triazole interact with different biological targets through complementary binding patterns, indicating their possible multimechanistic anticancer behaviour.

RMSD (root mean square deviation): The molecular dynamics simulations were performed for all four targets–β-tubulin (1SA0), caspase-3 (1PAU), PARP-1 (4R6E) and estrogen receptor α (3ERT) in both *apo* and ligand-bound states to evaluate structural stability, conformational changes and mechanistic relevance of the benzimidazole derivatives (Figs. 2-5). Across all systems ligand binding consistently improved structural stability relative to the *apo* forms demonstrating that each compound was well accommodated within its respective active pocket and maintained favourable interactions throughout the 100 ns trajectory.

Root mean square (RMS) fluctuation: The polymerisation loops of tubulin, the catalytic dyad zone of caspase-3, the NAD^+-binding cleft of PARP-1 and the activation helix of ERα are all functionally essential areas where ligand interaction regularly decreases flexibility. This decrease in local fluctuations after ligand binding shows that the benzimidazole derivatives strengthen stabilising connections that confine the proteins to conformational states that are detrimental to the development of cancer. Thus, the RMSF data show that the benzimidazole scaffolds can stabilise important functional domains across several targets, which is consistent with the expected inhibitory actions of the scaffolds.

TABLE-1
SUMMARY OF ALL THE SELECTED TARGETS AND THEIR CORRESPONDING DOCKING SCORES AND ACTIVE-SITE RESIDUES

Compound	Target	PDB ID:	Binding affinity (Kcal mol^{-1})	Interaction residues
5e	Target: β-Tubulin	1SA0	-4.11083	ASN101, ALA99, GLU71, THR145, GLY144, ASP179, GLN11, GLY143, CYS12, GLY142, SER140, VAL171, ASN206, PRO173, GLU183
7a	Caspase-3	1PAU	-4.81996	TRP B: 340, CYS A: 285, PHE B: 381H, TYR B: 338, SER B:339, ARG B: 341, ASN B: 342, SER B: 343
7b	PARP-1	4R6E	-6.31446	GLU988, TYR896, PHE897, ALA898, LYS903, SER904, TYR907, GLY863, HIS862, TRP861, TYR889
9a	Estrogen receptor modulation	3ERT	-6.85419	LEU428, LEU391, GLU353, ALA350, LEU349, LEU387, THR347, GLY521, LEU384, TRP383, LEU346, ILE424, HIS524, GLY420, PHE404, MET388, HIE524, LEU525, GLU419, MET421, ILE424, MET343, GLU419

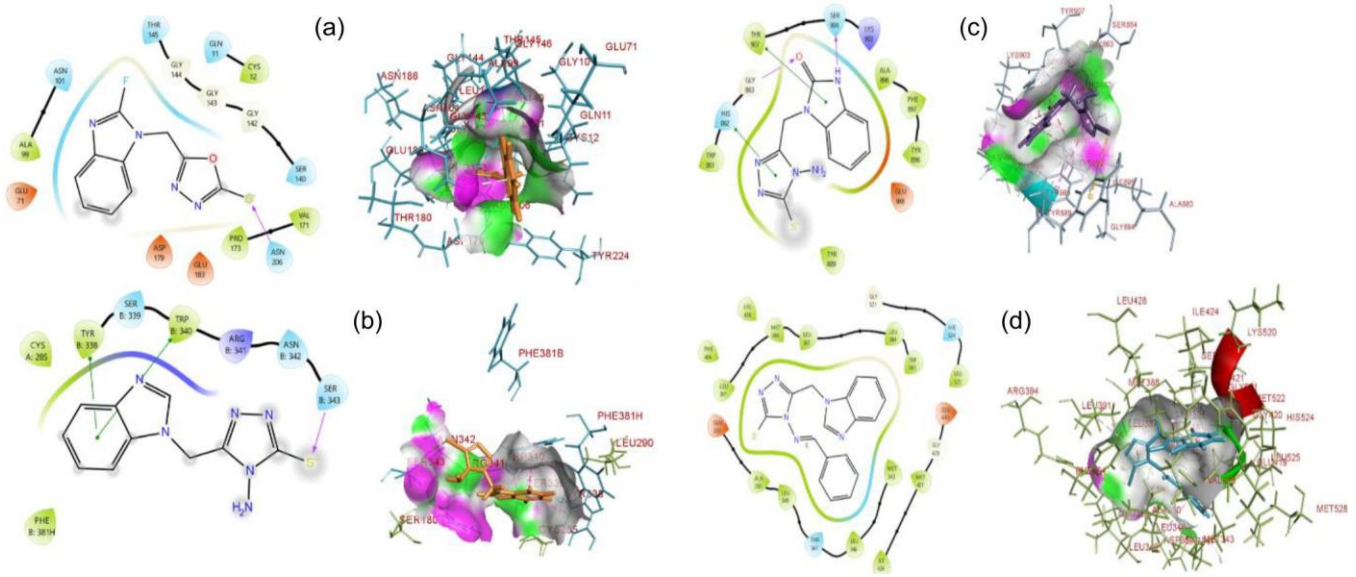

Fig. 1. Protein-ligand interaction poses of (a) 1SA0-**5e**, (b) 1PAU-**7a**, (c) 4R6E-**7b** and (d) 3ERT-**9a**

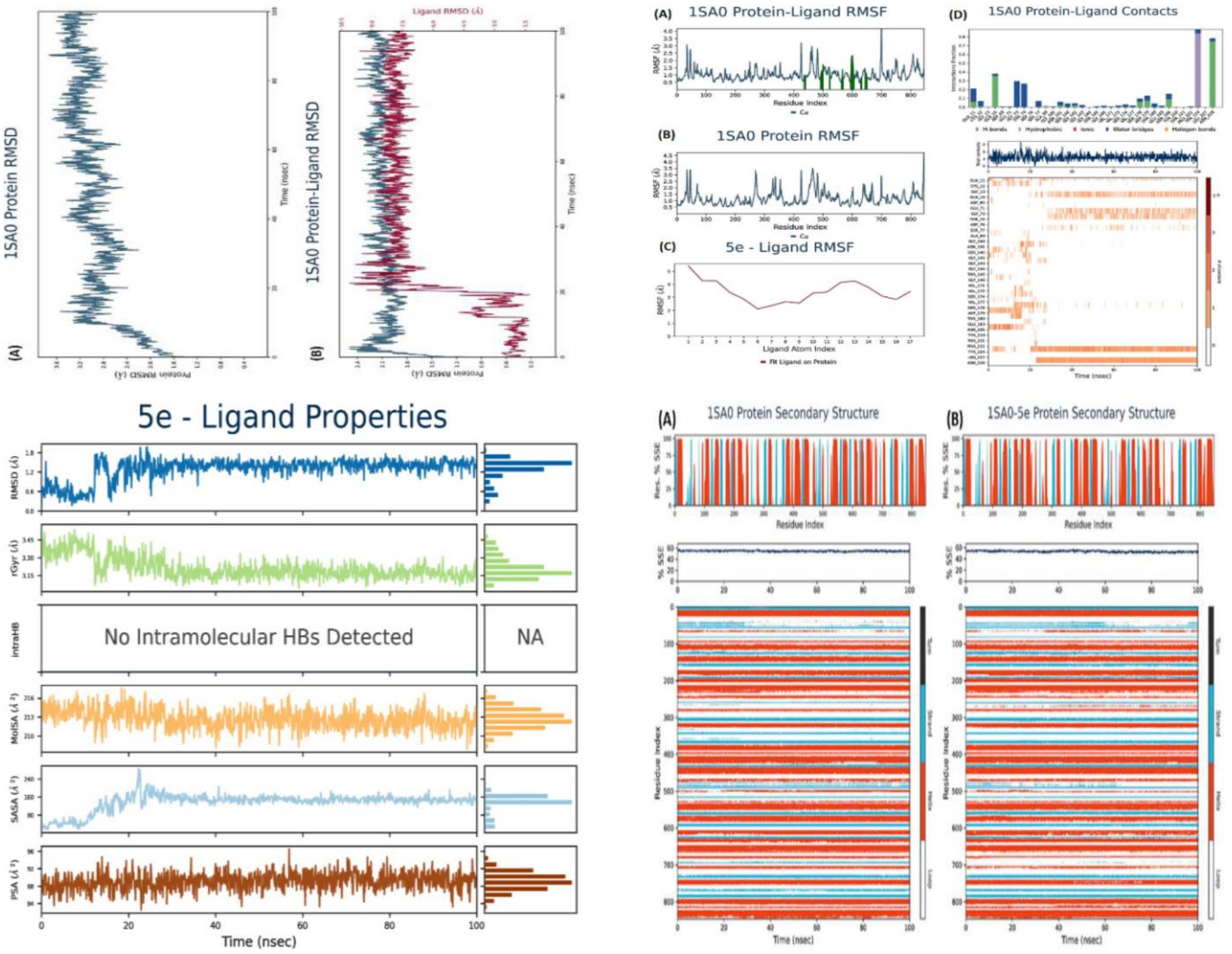

Fig. 2. Molecular dynamics analysis of β-tubulin in the absence and presence of compound **5e**; (A) RMSD of β-tubulin (1SA0); (B) RMSD of β-tubulin–**5e** complex; (C) RMSF of β-tubulin (1SA0); (D) RMSF of β-tubulin–**5e** complex; (E) RMSF of **5e**; (F) Protein–ligand interaction fraction and total contacts of the β-tubulin–**5e** complex; (G) Ligand properties of **5e**; (H) Secondary structure analysis of β-tubulin (1SA0) and β-tubulin–**5e** complex during the simulation time

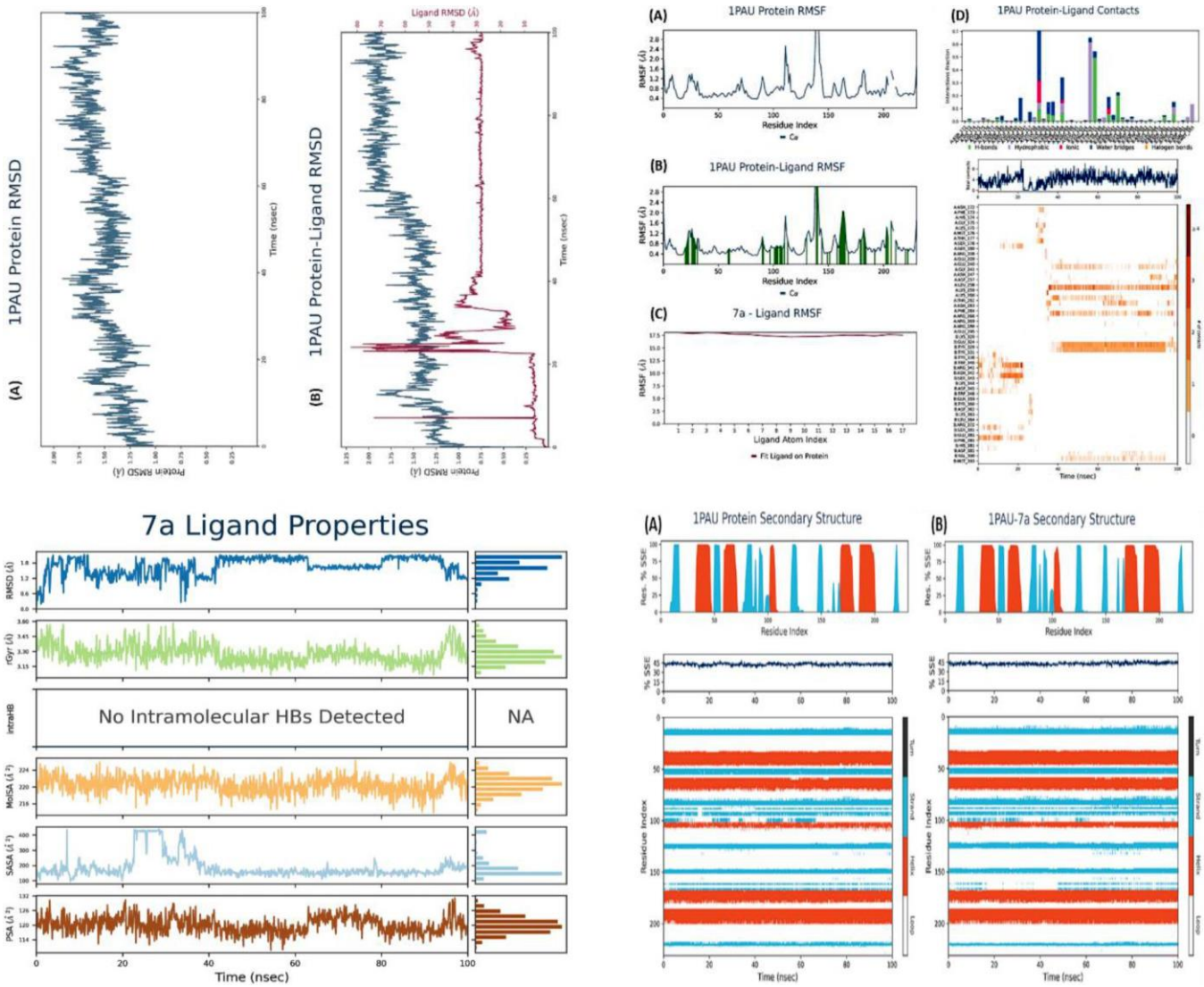

Fig. 3. Molecular dynamics analysis of caspase-3 (1PAU) in the absence and presence of compound **7a**; (A) RMSD of caspase-3 (1PAU); (B) RMSD of caspase-3–**7a** complex; (C) RMSF of caspase-3 (1PAU); (D) RMSF of caspase-3–**7a** complex; (E) RMSF of **7a**; (F) Protein–ligand interaction fraction and total contacts of the caspase-3–**7a** complex; (G) Ligand properties of **7a**; (H) Secondary structure analysis of caspase-3 (1PAU) and caspase-3–**7a** complex during the simulation time

Ligand properties: The ligand-properties analyses (rGyr, SASA and MolSA) showed consistent patterns across all four protein systems: β-tubulin, caspase-3, PARP-1 and oestrogen receptor α. All ligands (**5e**, **7a**, **7b**, **9a**) maintained a compact well-defined conformation without unfolding or solvent exposure as evidenced by the nearly consistent values of these parameters in each complex for the course of 100 ns trajectory. The combination of stable MolSA profiles (≈ 280-340 Å^2) modest SASA ranges (≈ 180-220 Å^2) and stable rGyr values (3.3-3.6 Å) indicates profound burial of each ligand within its corresponding binding cleft, little distortion and prolonged pocket retention. Long-term binding stability and energetically advantageous ligand–protein complementarity is strongly supported by these characteristics.

Interaction range: Throughout the simulation's hydrogen bonds, π–π stacking, hydrophobic contacts and occasional electrostatic interactions all helped the ligands maintain stable binding across all four targets. Across systems hydrogen-bond occupancies generally varied from ~0.5 to >0.6, indicating persistent polar anchoring. In the catalytic or regulatory pockets of caspase-3 and PARP-1, aromatic connections (π–π stacking) demonstrated >50% occupancy, while hydrophobic contacts especially in ERα and β-tubulin, showed >60% occupancy, indicating tight, densely packed binding environments. Pocket retention was further assisted by occasional water-mediated interactions as demonstrated by PARP-1. Thus, the interaction profiles demonstrate that every ligand continuously supported robust well-retained binding throughout all trajectories by maintaining high-occupancy multi-type interactions within its corresponding binding pocket.

Secondary structure analysis: Secondary-structure analyses revealed that ligand binding maintained the native α-helices and β-strands in all four complexes without inducing unfolding or destabilisation. The core structural components of tubulin, caspase-3, PARP-1 and ERα were all preserved suggesting that each ligand stabilises the protein rather

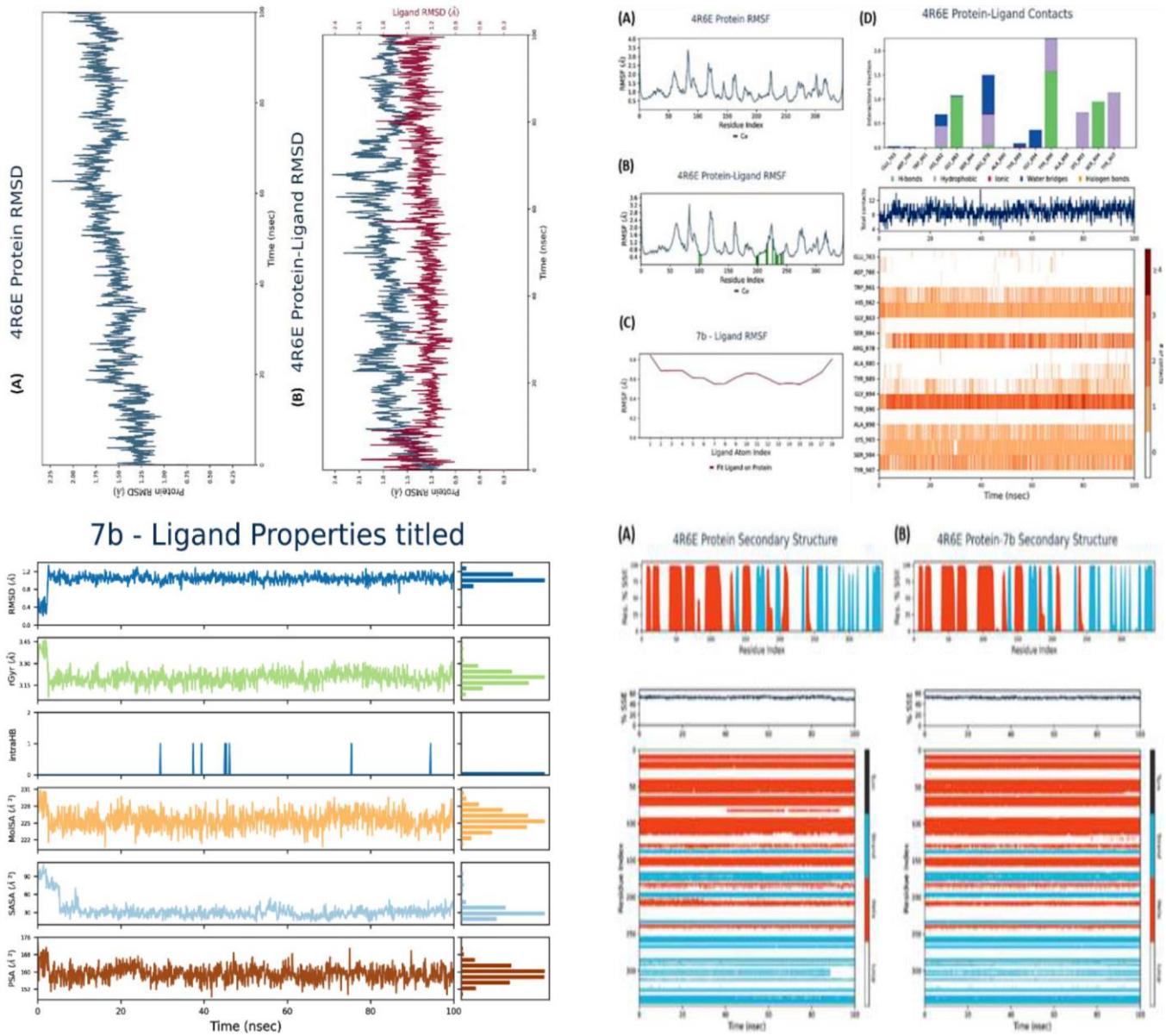

Fig. 4. Molecular dynamics simulation analysis of PARP-1 (4R6E) in the absence and presence of compound **7b**; (A) RMSD of PARP-1 (4R6E); (B) RMSD of PARP-1–**7b** complex; (C) RMSF of PARP-1 (4R6E); (D) RMSF of PARP-1–**7b** complex; (E) RMSF of **7b**; (F) Protein–ligand interaction fraction and total contacts of the PARP-1–**7b** complex; (G) Ligand properties of **7b**; (H) Secondary structure analysis of PARP-1 (4R6E) and PARP-1–**7b** complex during the simulation period

than altering its global fold. This structural consistency reinforces the stability and biological relevance of the ligand–protein complex.

Mechanistic correlation: Through different but complementary processes integrated molecular docking and molecular dynamics investigations together show the anticancer relevance of hybrids formed from benzimidazoles **5e**, **7a**, **7b** and **9a**. In accordance with microtubule-polymerisation inhibition compound **5e** (oxadiazole) successfully stabilised the colchicine binding region of β-tubulin, supported by hydrophobic interactions with VAL171 and PRO173 and sustained hydrogen bonding with ASN206. The strong interactions with caspase-3 and PARP-1 were demonstrated by triazole hybrids **7a** and **7b**, respectively: **7a** formed stable hydrogen bonds and π–π stacking with important apoptotic residues (TYR338, TRP340, SER343, ARG341), while **7b** replicated classical PARP inhibitor–like interactions in the NAD^+-binding cleft (SER904, GLY863, TYR907), supporting apoptosis activation and DNA repair suppression. Within the ERα hormone-binding pocket the Schiff-base derivative **9a** showed stable hydrogen bonding (GLU353, THR347) and dense hydrophobic packing (LEU349, MET388, LEU391), indicating stabilisation of an antagonist-like conformation related to ER^+ breast cancer. These results show that the benzimidazole scaffolds work by coordinating the manipulation of tubulin dynamics, apoptotic signalling, DNA repair inhibition and oestrogen receptor regulation. This suggests that the scaffolds have the ability to modulate several anticancer pathways. The summary of proposed biological mechanisms and molecular targets of the synthesised hybrid molecules is shown in Table-2.

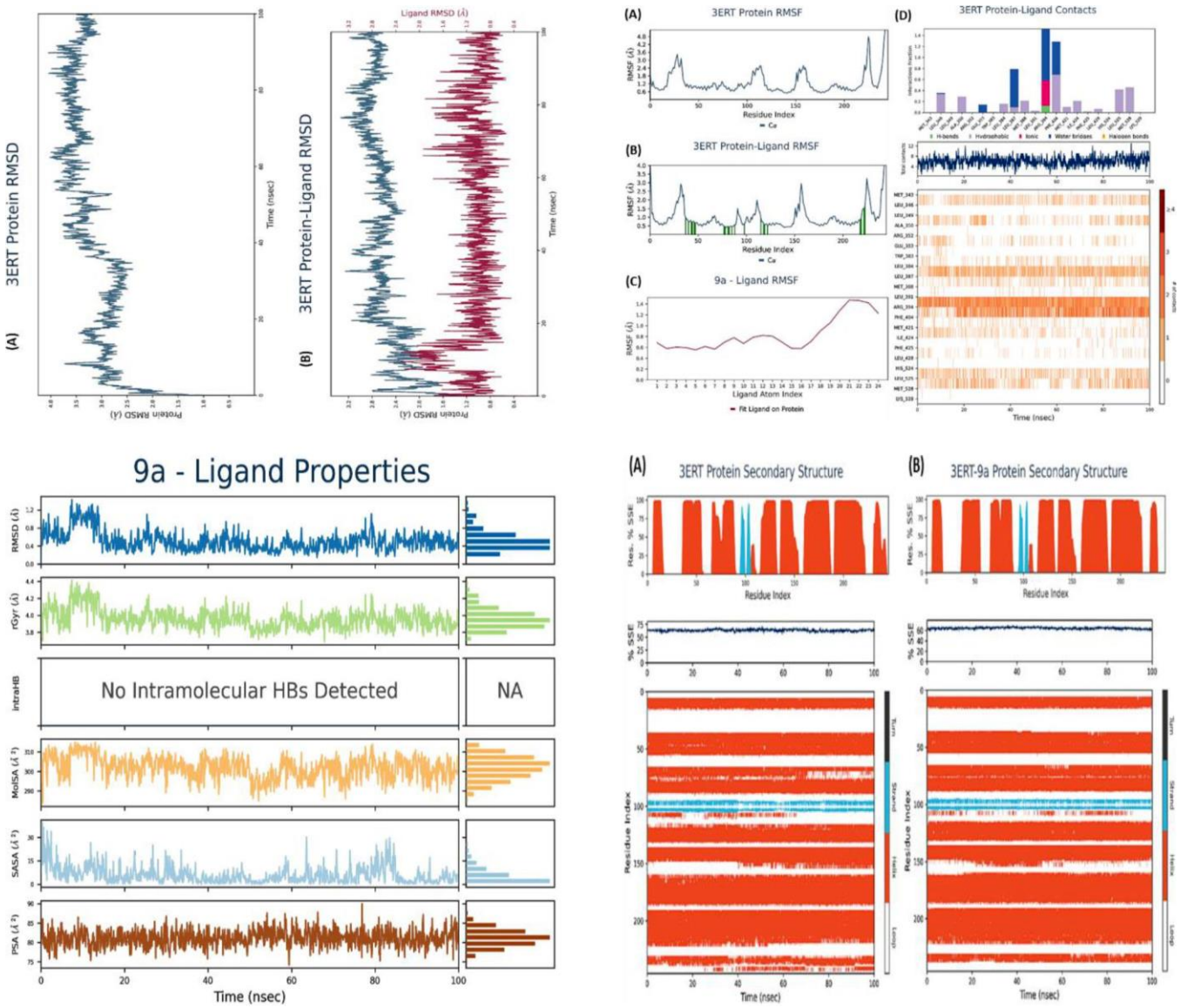

Fig. 5. Molecular dynamics simulation analysis of estrogen receptor (3ERT) in the absence and presence of compound **9a**; (A) RMSD of estrogen receptor (3ERT); (B) RMSD of estrogen receptor–**9a** complex; (C) RMSF of estrogen receptor (3ERT); (D) RMSF of estrogen receptor–**9a** complex; (E) RMSF of **9a**; (F) Protein–ligand interaction fraction and total contacts of the estrogen receptor–**9a** complex; (G) Ligand properties of **9a**; (H) Secondary structure analysis of estrogen receptor (3ERT) and estrogen receptor–**9a** complex during the simulation period

ADME and drug-likeness profiling: With balanced solubility permeability profiles (log P 0.17-3.7, PSA 55-104 Å^2) and minimal risk of CNS exposure all four compounds satisfied Lipinski criteria. Their promise as anticancer candidates are supported by the ADME data (Table-3), which generally show good oral viability and pharmacokinetic fit.

***In vitro* cytotoxicity studies:** The cytotoxic potential of the selected benzimidazole hybrids was assessed against MCF-7 cells using the MTT assay. Consistent with molecular docking results, compound **7a** exhibited the highest antiproliferative activity (IC_{50} = 8.7 ± 0.5 μM), which correlates with its superior docking score and stable hydrogen-bonding and hydrophobic interactions within the target binding site. The oxadiazole linked derivative 5e also showed significant activity (IC_{50} = 12.3 ± 1.1 μM), in agreement with its favourable binding orientation and key heteroatom-mediated interactions predicted *in silico*. Compound **7b** displayed moderate cytotoxicity (IC_{50} = 15.0 ± 2.0 μM), reflecting comparatively weaker binding interactions, while the Schiff base-containing triazole **9a** showed the lowest activity (IC_{50} = 22.1 ± 1.3 μM), consistent with its reduced docking affinity. Thus, the close agreement between *in vitro* cytotoxicity and docking results underscores the structural adaptability of the benzimidazole scaffold, wherein oxadiazole, triazole and Schiff base functionalities promote differential target engagement through complementary binding modes, supporting their potential multi-mechanistic anticancer behaviour.

Conclusion

A new series of benzimidazole derivatives incorporating 1,3,4-oxadiazole, 1,2,4-triazole and Schiff base moieties were

TABLE-2
SUMMARY OF PROPOSED BIOLOGICAL MECHANISMS AND MOLECULAR TARGETS OF THE DESIGNED HYBRID MOLECULES

Compound class	Proposed mechanism of action	Selected molecular target(s)	PDB ID	Biological rationale
Oxadiazole hybrids (**5a-g**)	Inhibition of tubulin polymerisation leading to mitotic arrest and cell-cycle disruption	β-Tubulin	1SA0	1,3,4-Oxadiazole derivatives are known for their anticancer potential *via* inhibition of tubulin polymerisation, disrupting microtubule dynamics and inducing apoptosis in proliferating cells [18,19].
Triazole hybrids (**7a-g**)	Induction of apoptosis and ROS-mediated cytotoxicity	Caspase-3, PARP-1	1PAU, 4R6E	Triazole-based scaffolds have been reported to activate intrinsic apoptotic pathways by modulating caspase-3 and PARP-1, resulting in DNA fragmentation and cell death [20-22].
Schiff base derivatives (**9a-g**)	Modulation of estrogen receptor (ER) signalling pathways	ERα	3ERT	Schiff-base compounds, particularly triaryl-substituted analogues, exhibit estrogen-receptor modulation and subtype-selective ligand behaviour, suggesting potential ERα binding and transcriptional control [23].

TABLE-3
SUMMARY OF PHYSICO-CHEMICAL PROPERTIES AND ADME PREDICTIONS FOR SELECTED TEST COMPOUNDS

Descriptor	Acceptable range	**5e**	**7a**	**7b**	**9a**	Notes
Molecular weight (Da)	130–725	250.25	246.289	262.289	334.398	Within optimal range
log P (QPlog Po/w)	–2.0 to 6.5	2.317	0.767	0.174	3.706	Balanced lipophilicity
Polar surface area (Å^2)	≤140	55.033	76.093	104.461	57.983	Good permeability
HBD/HBA	≤5/≤10	0.8/4	2.8/5.5	3.8/6	0.8/5	Within acceptable limits
QPlogS	–6.5 to 0.5	-3.148	-1.346	-1.34	-3.93	Acceptable aqueous solubility
QPlogBB	–3.0 to 1.2	-0.111	-0.159	-0.578	-0.32	Low CNS risk
Rule-of-five violations	≤1	0	0	0	0	Fully compliant
Human oral absorption (%)	0–100	3	2	2	3	High oral absorption potential

synthesised and evaluated for breast anticancer activities. The compound (**5e**) with electron-withdrawing group (–F), compounds (**7a**, **7b**) with electron-donating groups (–OH, -NH_2) substituents and Schiff base (**9a**) containing benzimidazole hybrid heterocyclic groups significantly influenced anticancer activity. Microtubule polymerisation inhibition was suggested the moderate binding of by oxadiazole hybrid **5e** to β-tubulin. While the Schiff base **9a** firmly bound ERα, confirming regulation of hormone-dependent signalling, triazole derivatives **7a** and **7b** interacted substantially with caspase-3 and PARP-1 indicating apoptosis activation and hindered DNA repair. QikProp ADME profile showed good drug-likeness, oral survivability and complete Lipinski compliance whereas MD simulations verified stable complexes with maintained secondary structures. All these studies considered these hybrids of benzimidazoles show promise as multifunctional antibacterial and anticancer agents.

ACKNOWLEDGEMENTS

The authors are thankful to the Yenepoya (Deemed to be University) for their direct and indirect support in completing this research work and providing chemicals and research facilities.

CONFLICT OF INTEREST

The authors declare that there is no conflict of interests regarding the publication of this article.

DECLARATION OF AI-ASSISTED TECHNOLOGIES

During the preparation of this manuscript, the authors used an AI-assisted tool(s) to improve the language. The authors reviewed and edited the content and take full responsibility for the published work.

REFERENCES

1. N. Xiong, H. Wu and Z. Yu, *Front. Oncol.*, **14**, 1405491 (2024); https://doi.org/10.3389/fonc.2024.1405491
2. P. Pastena, H. Perera, A. Martinino, W. Kartsonis and F. Giovinazzo, *Int. J. Mol. Sci.*, **25**, 2559 (2024); https://doi.org/10.3390/ijms25052559
3. D.K. Singh, H. Iqbal and M.A. Ansari, *Curr. Org. Chem.*, **28**, 733 (2024); https://doi.org/10.2174/0113852728303189240321084818
4. K. Mahmood, Z. Akhter, F. Perveen, M. Bibi, H. Ismail, N. Tabassum, Aisha, S. Yousuf, A.R. Ashraf and M.A. Qayyum, *RSC Adv.*, **13**, 11982 (2023); https://doi.org/10.1039/D3RA00982C
5. F. Vitali, L.D. Cohen, A. Demartini, A. Amato, V. Eterno, A. Zambelli and R. Bellazzi, *PLoS One*, **11**, e0162407 (2016); https://doi.org/10.1371/journal.pone.0162407
6. W.R. Mir, B.A. Bhat, A. Kumar, R. Dhiman, M. Alkhanani, M.Y. Dar, A. Almilaibary, S.A. Ganie and M.A. Mir, *Front. Pharmacol.*, **14**, 1135898 (2023); https://doi.org/10.3389/fphar.2023.1135898
7. A. Kamal, A.B. Shaik, S. Polepalli, V. Santosh Reddy, G. Bharath Kumar, S. Gupta, K.V.S. Rama Krishna, A. Nagabhushana, R.K. Mishra and N. Jain, *Org. Biomol. Chem.*, **12**, 7993 (2014); https://doi.org/10.1039/C4OB01152J
8. A. Vaidya, D. Pathak and K. Shah, *Chem. Biol. Drug Des.*, **97**, 572 (2021); https://doi.org/10.1111/cbdd.13795

9. A.M. Abdelhakem and M.N. El-Shimaa, *Octahedron Drug Res.*, **60**, 112 (2024).
10. N. Kulabaş, E. Tatar, Ö. B. Özakpınar, D. Özsavcı, C. Pannecouque, E. De Clercq, and İ. Küçükgüzel, *Eur. J. Med. Chem.*, **121**, 58 (2016); https://doi.org/10.1016/j.ejmech.2016.05.017
11. T. Mondal, A.V.S. Lavanya, A. Mallick, T.L. Dadmala, R.M. Kumbhare, U. Bhadra and M.P. Bhadra, *Apoptosis*, **22**, 786 (2017); https://doi.org/10.1007/s10495-017-1367-1
12. Z.Q. Liao, C. Dong, K.E. Carlson, S. Srinivasan, J.C. Nwachukwu, R.W. Chesnut, A. Sharma, K.W. Nettles, J.A. Katzenellenbogen and H.B. Zhou, *J. Med. Chem.*, **57**, 3532 (2014); https://doi.org/10.1021/jm500268j
13. B. Nabuurs, M. Wagener and J. de Vlieg, *J. Med. Chem.*, **50**, 6507 (2007); https://doi.org/10.1021/jm070593p
14. G.M. Sastry, M. Adzhigirey, T. Day, R. Annabhimoju, W. Sherman, *J. Comput. Aided Mol. Des.*, **27**, 221 (2013).
15. R.C. Johnston, K. Yao, Z. Kaplan, M. Chelliah, K. Leswing, S. Seekins, S. Watts, D. Calkins, J. Chief Elk, S.V. Jerome, M.P. Repasky and J.C. Shelley, *J. Chem. Theory Comput.*, **19**, 2380 (2023); https://doi.org/10.1021/acs.jctc.3c00044
16. R.A. Friesner, J.L. Banks, R.B. Murphy, T.A. Halgren, J.J. Klicic, D.T. Mainz, M.P. Repasky, E.H. Knoll, M. Shelley, J.K. Perry, D.E. Shaw, P. Francis and P.S. Shenkin, *J. Med. Chem.*, **47**, 1739 (2004); https://doi.org/10.1021/jm0306430
17. Z. Kaplan, S. Ehrlich and K. Leswing, Benchmark Study of DeepAuto-QSAR, ChemProp and DeepPurpose on the ADMET Subset of the Therapeutic Data Commons, Schrödinger, Inc. (2022); https://www.schrodinger.com/wpcontent/uploads/2023/10/22_086_machine_learning_white_paper_r4-1.pdf
18. A.S. Shokouhi Asl, S. Ranjbar, M.H. Sayahi, Z. Dehghani, M. Emami, A.M. Taherkhani, M. Negahdaripour, N. Dastyafteh, S. Safapoor, A. Ghahramani, M.R. Mohajeri-Tehrani, B. Larijani, M. Mahdavi and Y. Ghasemi, *RSC Adv.*, **15**, 37447 (2025); https://doi.org/10.1039/D5RA02760H
19. A.M. Malebari, M.A.M. Ali, A. Musa, M.E.A. Zaki, S.M. Gomha, M.A. Soliman, M.A. Abdelgawad, D.G.T. Parambi, M.R. Aouad, H.S. Abulkhair and H.E.A. Ahmed, *RSC Adv.*, **15**, 47601 (2025); https://doi.org/10.1039/D5RA07972A
20. B. Huwaimel, A.S. Abouzied, M.E.A. Zaki, A. Alamri, B. Farag, S. Alqarni and S.M. Gomha, *ChemistryOpen.*, **14,** e202500288 (2025); https://doi.org/10.1002/open.202500288
21. M.N. El-Bayaa, A.M. Srour, A.L. Alanzy, S. Messaoudi, A.A. Abd-Rabou, A. Saleh, M.G.A. Saleh and W.A. El-Sayed, *Future Med. Chem.*, **17**, 2927 (2025); https://doi.org/10.1080/17568919.2025.2587567
22. A.M. Srour, M.N. El-Bayaa, A. Temirak, A.L. Alanzy, H.M. Awad, A. Saleh, M.G. Saleh and W.A. El-Sayed, *Sci. Rep.*, **15**, 25514 (2025); https://doi.org/10.1038/s41598-025-96675-3
23. S. Alqahtani, M.A. Al-Omar, H.A. Ghabbour and A.A. El-Emam, *Molecules.*, **28**, 4123 (2023); https://doi.org/10.3390/molecules28104123